Research Article / Review Article FUPRE JOURNAL 9(2):124-134(2025)

FUPRE Journal

of

Scientific and Industrial Research

ISSN: 2579-1184(Print) ISSN: 2578-1129 (Online)

http://fupre.edu.ng/journal

Investigating the structural, optical and electrical properties of electrochemically deposited aluminum-doped manganese sulfide for photovoltaic applications

***IJEH, R.*[*,1], IMOSOBOMEH, L.*[2]**

[1]*Department of Physics, University of Delta, Agbor, Nigeria*
[2]*Department of Physics, Federal University Lokoja, Kogi State, Nigeria*

ARTICLE INFO

Received: 20/03/2025
Accepted: 23/07/2025

Keywords

Bandgap, Doping, Molarity, Structural, Optical, Semiconductor

ABSTRACT

MnS has garnered considerable research attention because of its interesting magneto-optical properties, layered structure and superior charge transport facilitated by ionic strength. The micrographs revealed that Al doped MnS resulted to agglomeration from rod like shapes to uniform spherical nanostructures. The XRD analysis of MnS reveals a cubic crystal structure, evidenced by distinct peaks. The pattern of MnS is modified by the addition of aluminum due to Mn ion replacement resulting to subtle peak position and intensity changes. The energy bandgap decreased from 2.30 to 2.22 eV as the concentration increased from 0.1 to 0.3 M. The results obtained from the four-point probe showed that as the electrical resistivity increased from 0.126 to 0.142 ohm/m, the resulting conductivity reduced from 7.935 to 7.042 S/m. The deposited thin films can be applied for photovoltaic and solar cells applications.

1. INTRODUCTION

Growing populations and increased daily energy consumption have driven a dramatic rise in renewable energy demand. Despite its weather dependency, it is relatively abundant, clean, and environmentally friendly. Fossil fuels' drawbacks have spurred research into efficient, stable semiconductor materials for photovoltaic applications. Semiconductors are key materials in the electronics industry, essential for amplifying signals and producing chips that underpin economic progress. As electronic products, advanced computer chips for connectivity and robotics underpin scientific and technological trade, boosting economic development. Recent advancements in semiconductor materials production will improve data transfer in AI-integrated memory circuit systems (Licardo et al., 2024; Liu et al., 2024). The layered structure, high electron mobility, and tunable optoelectronic properties (bandgaps) of Transition Metal Chalcogenides (TMCs) have made them recent research topics. The non-volatile nature and chemical stability of most TMC also make them very promising materials (Hassanzadeh et al., 2015; Zhao et al., 2021).

Due to its abundance and technological relevance, manganese sulfide (MnS), a widely studied metal sulfide, absorbs long-wavelength light. MnS has attracted significant research interest due to its

*Corresponding author, e-mail: rufus.ijeh@unidel.edu.ng, ikhioyalucky@gmail.com
DIO

exciting magneto-optical properties, layered structure, and optimal charge transport enabled by ionic strength. The wide bandgap of manganese sulfide thin films, an important binary IV–VI semiconductor material, measures 3.84 to 4.29 eV (Ijeh et al., 2023). MnS is well-suited as a solar cell absorber layer due to its wide band gap. Zheng et al. (2006) demonstrated this magnetic semiconductor's efficacy across spintronics, optoelectronics, photochemistry, and other relevant applications. Due to their high electrical conductivity, porous structure, optoelectronic properties, and catalytic activity for hydrogen production in water splitting, manganese sulfide semiconductor materials are efficient and ideal electrode materials for energy storage devices and batteries (Imran et al., 2023). A semiconductor's Fermi level and band gap are altered by incorporating ferromagnetic manganese (Mn^{+2}) into its lattice. Manganese salt, upon complexing agent introduction, yielded Mn^{2+} and S^{2-} ions, thus resulting in low Mn^{2+} ion levels.

Semiconductor bandgap engineering seeks to align with solar wavelengths, boosting light absorption for better crystal electronics (Miah et al., 2024).

Three polymorphs exist for MnS: α-MnS (cubic rock-salt), β-MnS (zinc blende), and γ-MnS (wurtzite), the latter being prone to transformations. Despite the high stability of α-MnS above room temperature, β-MnS and γ-MnS are only metastable. Low temperatures allow convenient transformation of the metastable phase into the α-phase; above 200°C, the γ-phase also transforms into the α-phase (Zhang et al., 2018). According to Petrakovsk et al. (2001), the surface arrangement of α-MnS forms a face-centered crystal structure where the magnetic moments show a ferromagnetic alignment with the planes and antiferromagnetic alignment within the plane, whereas β- and γ-MnS have a tetrahedral arrangement. Temperature is thus undeniably a major factor in the electronic band theory of materials, particularly polymorphic ones like manganese sulfide. Manganese sulfide thin film synthesis uses several deposition techniques, such as chemical bath deposition (Chaki et al., 2017; Yu, et al., 2013), hydrothermal (Zhang et al., 2002), microwave (Wang et al., 2005; Jeyamalar and Selvarajan, 2021), spray pyrolysis (Chowdhury et al., 2011), SILAR (Moreno-García et al., 2024; Pathan et al., 2007), thermal vacuum evaporation (Hannachi et al., 2016) and reactive sputtering technique (Tiwari et al., 2019). Compared to other deposition methods, electrochemical deposition excels in MnS thin film synthesis, offering a fast, inexpensive, reliable process for large-area films at room temperature (Imran et al., 2023).

Doping alters the band gap (e.g) and Fermi level of materials, especially thin films in order to improve their electrical, optical, and mechanical characteristics. The primary goal of this study is to ascertain how dopant influences crystal quality for the best possible application in films and technologies. Amri et al. (2023) produced aluminum-doped ZnO using the sol–gel dip-coating method. Results indicate a 3.26 eV band gap, 0.191 Ωcm resistivity, and >90% transmittance. This implies its use in optoelectronics. Aoun et al. (2015) used spray pyrolysis to make aluminum-doped ZnO with different levels (0–3%) of dopant. An 85% optical transparency was observed, with a bandgap energy of 3.281 eV. Abdulmunem et al. (2020) used vacuum evaporation to synthesize aluminum-doped zinc oxide. Optical analysis showed that the crystallite size was smaller, the band gap was lower, and transmittance was reduced. Utilizing sol-gel spin coating, Ghazai et al. (2016) produced Al-doped ZnO thin films. The films showed polycrystalline hexagonal wurtzite structures

with reduced lattice parameters. Increasing the dopant concentration decreased the bandgap energy from 3.37 to 3.25 eV.

Al-doped CuS was deposited using dual solution synthesis by Onwuemeka et al. (2024). Visible region transmittance ranged from 0.3% to 0.6%, reflectance from 0.176 to 0.204, and the estimated band gap energy was 2.6 eV. It is undeniable that researchers have made progress in enhancing the photovoltaic performance of manganese sulfide through the use of aluminium doping to optimize charge transport. This research is unique because, although many studies have been conducted on aluminum-doped metal oxides or sulfides, there's no evidence of effective research on electrodeposited aluminum-doped manganese sulfide to determine its morphological, electrical, and optical properties for photovoltaic applications.

Existing research on MnS doped with Al focused on energy storage applications. This study used aluminum-doped manganese sulfide thin films to enhance their structural and optical properties for photovoltaic and other technological applications. However, additional research will compare the morphological, electrical, and optical properties of various deposition methods to determine the best for photovoltaic applications.

2. EXPERIMENTAL DETAILS FOR ELECTROCHEMICAL DEPOSITION OF MNS AND AL DOPED MNS

2.1 Materials Required

Manganese (II) sulfate monohydrate ($MnSO_4.H_2O$), ammonium sulfide ($(NH)_2S$), aluminum sulfate hydrate, $Al_2(SO_4)_3 \cdot H_2O$, distilled water or a suitable buffer solution, conductive materials-fluorine doped tin oxide (FTO), Three-electrode setup (working electrode, graphite electrode, Saturated calomel electrode (SCE) as reference electrode), Voltage regulator (-0.5 V to -1.0 V vs. SCE) and a controlled current density (1-10 mA/cm²). The electrochemical bath system primarily consists of the cation source ($MnSO_4.H_2O$ $Al_2(SO_4)_3 \cdot H_2O$) for Mn^{2+}, Al^{2+}), the anion's sources (ammonium sulfide $(NH)_2S$ for S^{2-}). A conducting glass cathode and a copper anode were used, with a DC power supply providing the electric field. We finally achieved homogenous film deposition through electrochemical deposition.

2.2 Preparation of Electrolyte Solution and deposition

The 2.7 cm × 1.7 cm FTO substrate was cleaned thoroughly using ultrasonic cleaning in ethanol, acetone and distilled water (DM). Manganese salt (0.1 M), sulfide salt (0.1 M), aluminum salt (0.1 to 0.3 M) were added to 150 ml of DM and add a three drops of HCl to enhance the deposition. Three-electrode setup (working electrode (FTO), graphite electrode, saturated calomel electrode (SCE) as reference electrode), and a working electrode serving as the cathode. During every deposition, the chambers were filled with vertically oriented FTO-coated substrates, which housed the counter and reference electrodes. Films were cleaned and dried with a hand dryer after deposition. In the deposition process, 15 ml of Manganese (II) sulfate monohydrate ($MnSO_4.H_2O$) and ammonium sulfide ($(NH)_2S$) solutions (equal amounts) along with 5 ml of aluminum sulfate hydrate, $Al_2(SO_4)_3 \cdot H_2O$ solution were added to the beaker containing the target materials. Following deposition, samples underwent a 40-minute anneal in order to remove internal stress. A constant 10 V applied to the power supply. The optical, structural, elemental, and electrical properties of the synthesized materials were thoroughly analyzed with specialized tools and mathematical models. Absorbance measurements were obtained with a model 756s UV-V is spectrophotometer, covering 300-1100 nm. The structural analysis was conducted using an X-ray diffractometer, model cu-kal (λ = 1.15418Â). This method

gives in-depth information about crystal lattice properties, diffraction peak strength, and the crystal structures found in materials, both natural and man-made. The JEOL JSM 6360 SEM provided morphology data, and EDXs analysis provided chemical composition data. The film's thickness was determined with a surfacing/thicknessing mortise machine. The vintage Jandel four-point probe technique was finally used to examine the synthesized materials' electrical properties.

3. RESULTS

3.1 Optical study of Al doped MnS

MnS and Al-doped MnS are synthesized for optoelectronic and photovoltaic applications as shown in Figure 1a. The semiconductor nature of MnS leads to significant UV-Vis absorption. Aluminum doping alters MnS's electronic structure, resulting in absorption peak shifts. Al ion incorporation into the MnS lattice changes its bandgap. Incorporation of aluminum boosts visible-light absorbance via the generation of extra energy levels within the material's bandgap. Increasing Al doped MnS concentration from 0.1 to 0.3 M leads to higher absorbance because more species absorb light. Increased scattering and particle interactions at higher concentrations cause peak broadening in the absorbance spectra. Absorbance levels are off at a certain concentration when the solution becomes saturated, and additional increase in concentration results in diminishing returns in absorbance. The patterns seen in absorbance spectra indicate variations in concentration, doping effects, and material properties, all essential for enhancing their application in electronic and optoelectronic devices.

Figure 1b shows that the strong absorption of MnS in the visible region leads to its relatively low transmittance as a semiconductor. As the wavelength nears the fundamental absorption edge (400-500 nm), transmittance drops sharply. A sharp decrease in transmittance marks the fundamental absorption edge, where strong absorption starts. Aluminum doping in MnS changes its electronic structure, possibly affecting its transmittance. Introducing Al ions generates new energy levels inside the bandgap, affecting light absorption and transmission. Al doped MnS's transmittance increases in certain spectral regions, especially visible light, depending on the doping concentration, because of altered band structures. Increasing the Al doped MnS concentration from 0.1 to 0.3 M should reduce transmittance because of the increased absorption by the larger number of particles. Increased concentrations lead to broader absorption features, thus lowering transmittance within the relevant wavelengths. High material concentrations lead to a saturation point, where increased concentration doesn't significantly improve transmittance, as absorption effects prevail. Observed transmittance spectral trends are key to optimizing electronic and optoelectronic devices because they reveal the impact of concentration, doping and material characteristics.

Figure 1c shows the high absorption of MnS, stemming from its semiconducting properties and resulting in low reflectance in the visible and near-infrared spectral regions. As wavelengths approach the fundamental absorption edge (400-500 nm), the reflectance spectra shows decreased reflectance and increased absorption. Aluminum doping changes MnS's electronic structure, thus affecting its reflectance. Al ion inclusion alters surface morphology and electronic states, thus changing light-material interactions. Al doped MnS's reflectance in certain spectral regions, especially the visible range, rises with varying doping concentrations due to altered band structures and surface properties. Reflectance falls as MnS and Al doped MnS concentration rises

from 0.1 to 0.3 M which is due to increased light absorption by the greater number of particles. Increased particle density at higher concentrations enhances scattering, reducing reflectance. Above a certain high concentration, the material saturates and increasing its concentration has little effect on reflectance, because absorption is the primary process. Reflectance spectra trends to reveal concentration shifts, doping impacts and material properties crucial for optimizing electronic and optoelectronic device applications.

MnS has a band gap energy of about 2.75 eV. Figure 1d shows that significant UV-visible absorption in MnS highlights its semiconductor nature, suggesting its suitability for many optoelectronic applications. By introducing additional energy levels to its band structure, aluminum doping in MnS modifies its bandgap energy. The material's capacity for absorption increased as the effective bandgap energy dropped. This tendency can be explained by a bandgap narrowing brought on by the increased aluminum concentrations, which introduce more charge carriers. As the concentration rises from 0.1 to 0.3 M, the effective bandgap drops from 2.30 to 2.22 eV due to the additional energy levels via doping. According to the research, Al doped MnS can now absorb longer wavelengths of light, which may improve the efficiency of solar cells and photodetectors. The Al doped MnS's with decreased bandgaps enhance the electrical conductivity which makes it perfect for a variety of electronics applications, including transistors and sensors. The bandgap energy decreases with increasing aluminum concentration, highlighting the tunable optical and electrical capabilities of MnS for optoelectronics and semiconductor technology.

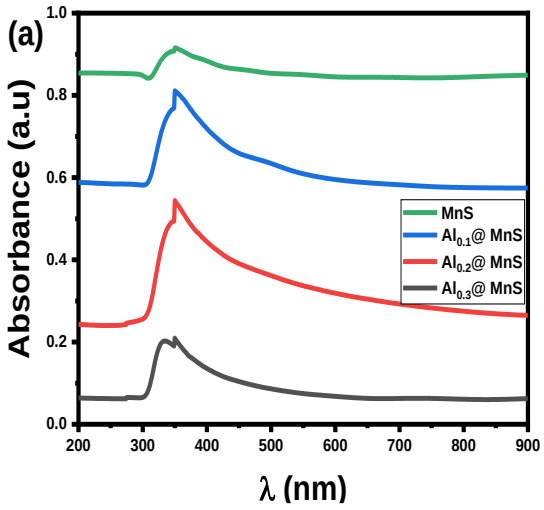

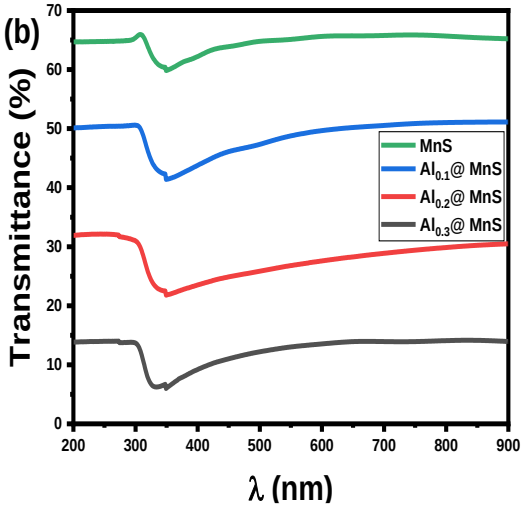

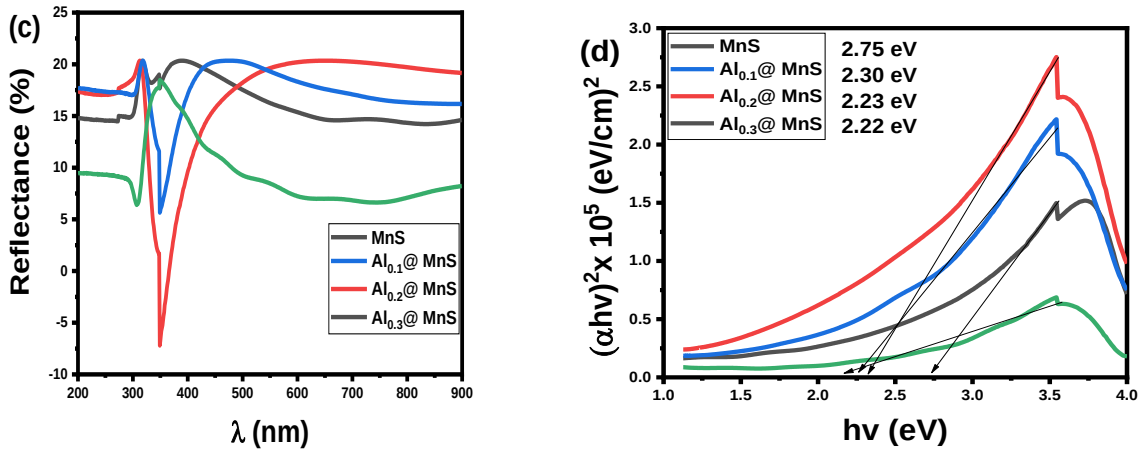

Figure 1: (a) arbitrary unit absorbance, (b)% transmittance, (c)% reflectance, (d) energy bandgap of Al @ MnS

3.2 Structure study of Al @ MnS

The impact of Al doping on the phase, crystallinity and structure of MnS at varying concentrations is investigated in this work. The XRD pattern shows distinct peaks that indicate a cubic crystal structure. The (100), (110), (111), and (200) planes shows where diffraction peaks can be found. Peak positions validate the material phase and lattice characteristics. Adding aluminum to the MnS structure alters its XRD pattern because aluminum ions replace manganese ions, which subtly shift peak positions and intensities. Doping-induced lattice strain broadens the XRD peaks and increased lattice strain and crystal disorder. New peaks appear with varying doping levels, signifying the creation of secondary phases. Higher concentrations lead to phase separation or new crystalline phases as evidenced by extra peaks in the XRD pattern. Crystallinity is reflected in the sharpness and intensity of the peaks. Peaks that are broader suggest less crystallinity, while sharper peaks indicate well-ordered structures. Phase identification in samples is achieved by comparing the observed peaks with standard reference patterns. XRD patterns show the crystalline structure, phase composition and effects of Al-doped MnS samples at different concentrations. Doping effects on the material's structural properties are shown by the concentration-dependent changes in peak positions, intensities, and broadening.

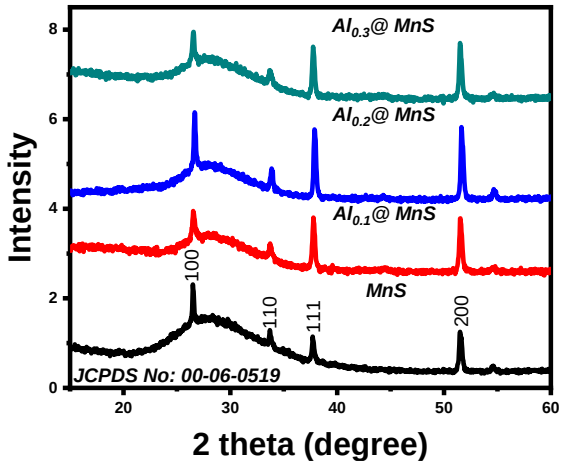

Figure 2: Structural pattern of Al doped MnS

3.3 Surface micrograph of Al doped MnS

In Figure 3, MnS surfaces are shown to have spherical nanoparticles, nanostructures, elongated shapes and rod-like structures. Spherical particles, with reduced size, increases the surface area to more elongated shapes. There's more particle agglomeration from rod like shapes to well defined spherical

nanostructures. Potentially networked or clustered structures of increased size and complexity. Introducing aluminum into the host of MnS alters growth kinetics and morphology via defect formation thereby affecting the size and shape. In comparism with the undoped MnS, Al (0.1 M)-doped MnS exhibits slightly larger particles, which results from enhanced stability and a more uniform particle distribution. Higher Al concentration (0.2 M) led to increased nanoparticle clustering and surface roughness. The Al (0.2 M) solution displays enhanced structural complexity, agglomeration, crystallinity, and potentially improved electronic properties resulting from doping. The surface roughness of Al-doped MnS is greater than that of undoped MnS, especially for higher doping levels. Higher doping concentrations lead to slightly larger particles because nucleation and growth are sped up. Improving MnS's structural stability and resistance to environmental changes is achieved through Al doping. The surface features of MnS and its aluminum-doped form change depending on the concentration of aluminum.

The EDX analysis of manganese sulfide (MnS) and aluminum-doped MnS mainly shows manganese (Mn) and sulfur (S) in Figure 4. EDX spectral analysis reveals significant peaks for manganese and sulfur, suggesting their presence in the sample at stoichiometric levels. EDX spectra, in addition to Mn and S, indicate aluminum (Al). Elemental distribution is changed by Al. Mn, S, and Al peaks appear, although Al peaks are weak because of its low doping concentration. Stronger Al peaks show more aluminum is in the MnS matrix. Prominent Mn, S, and Al peaks confirm substantial doping. The addition of Al altered the Mn/S ratio, suggesting potential new phases or compounds. Increased structural defects from doping cause enhanced peak broadening. EDX data shows elemental ratios shift with higher concentrations, suggesting MnS stoichiometry is impacted by doping. The presence of Aluminum changes the EDX spectra, showing altered peak intensities and positions indicating compositional and structural changes.

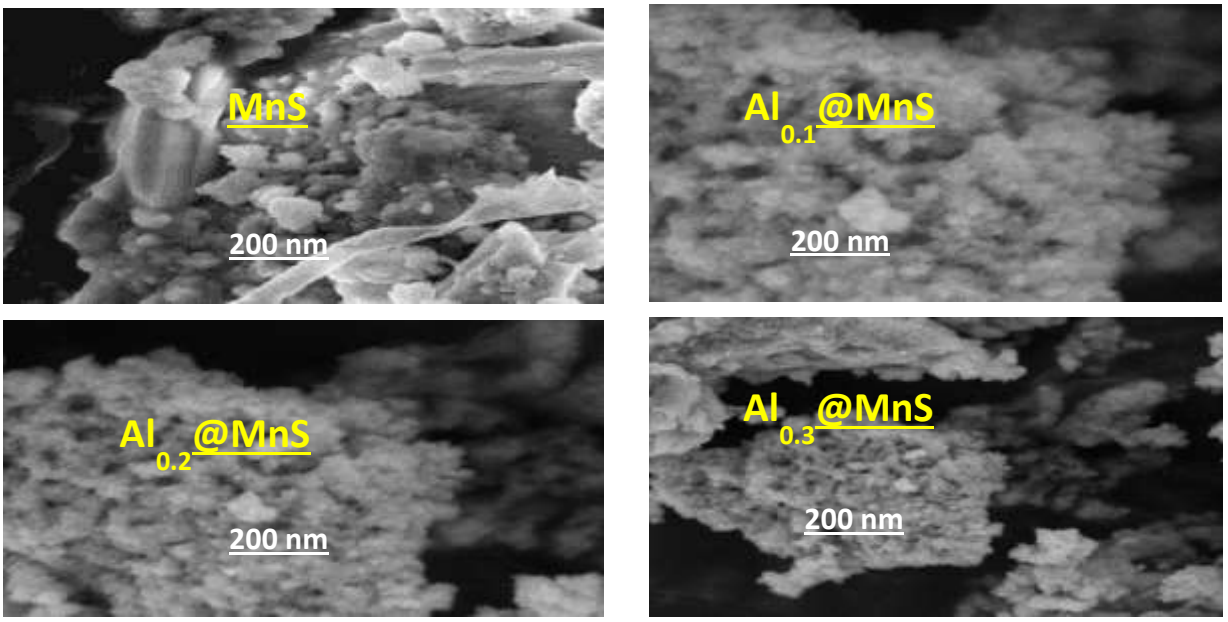

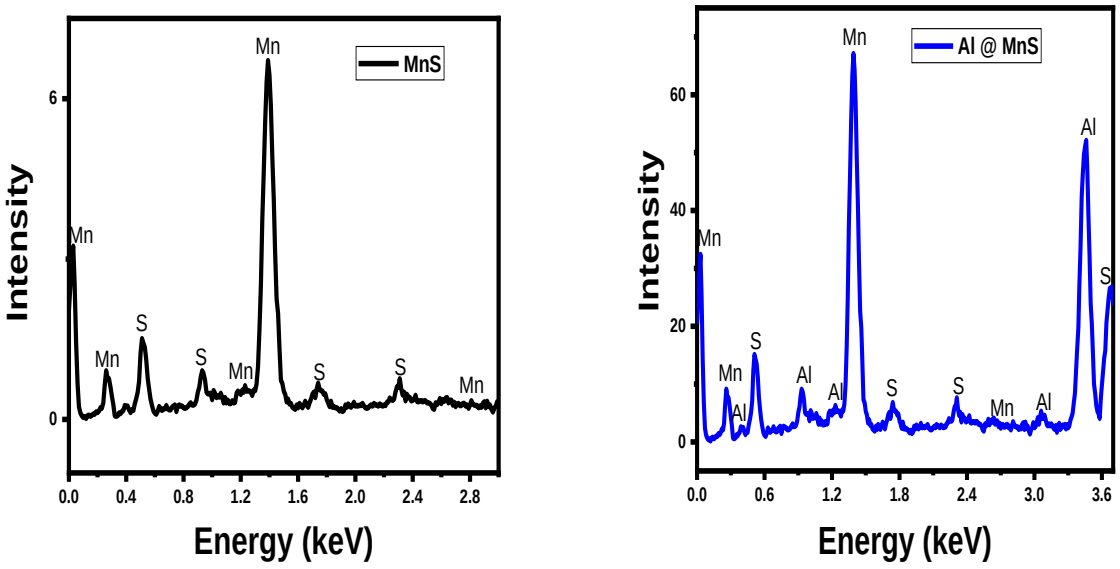

Figure 4: EDX spectrum of Al @ MnS

Table 2: Atomic percentage weight

MnS		Al@MnS	
Elements	A.W (%)	Elements	A.W (%)
Mn	75.70	Mn	74.70
S	24.30	S	10.15
-	-	Al	15.15

3.4 The electrical features of Al doped MnS

Resistivity and conductivity values for MnS and Al doped MnS are shown in Table 3. A decrease in film thickness from 107.07 to 103.13 nm led to a rise in resistivity from 0.126 to 0.142 ohm/m, resulting in a conductivity drop from 7.935 to 7.042 S/m. These deposited films are perfect for photovoltaic and solar cells due to their low resistivity and high conductivity. A non-linear graph illustrates the relationship between resistivity, conductivity, and film thickness. With high resistivity, conductivity decreases with the film thickness as depicted in Figure 5. A clear graph displays the correlation between resistivity, conductivity, and the changes in aluminum molarity.

Table 3: Electrical feature of Al @ MnS

Materials	Thickness, t (nm)	**ρ** (Ω.m) x 10^6	**σ** (S/m) x 10^6
MnS	107.07	0.126	7.935
$Al_{0.1@}MnS$	110.02	0.134	7.462
$Al_{0.2@}MnS$	104.54	0.139	7.194
$Al_{0.3@}MnS$	103.13	0.142	7.042

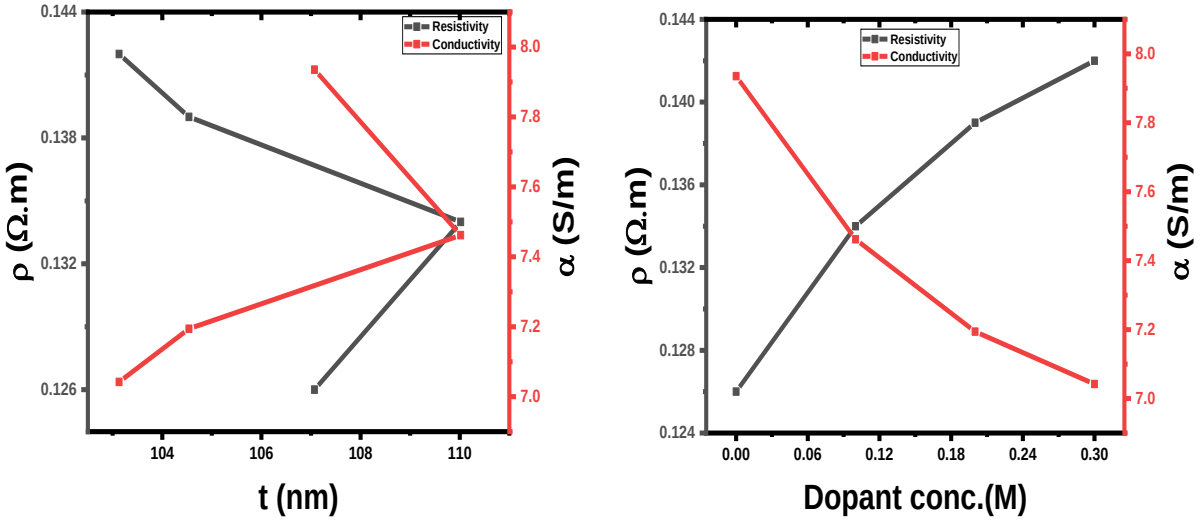

Figure 5: Resistivity and conductivity Vs thickness and dopant concentration of Al @ MnS

References

Abdulmunem, O.M., Ali, M. J. M., Hassan, E. S. (2020). Optical and structural characterization of aluminium doped zinc oxide thin films prepared by thermal evaporation system *Optical Materials* 109, 110374 https://doi.org/10.1016/j.optmat.2020.110374

Ali, H.M., Shokr, E.K., Ismail, A.A., Kamel, M.S., Mohamed, H.A., Hasaneen, M.F. (2024). Doping and precoating by Cu-metal and annealing impacts on some physical properties and applications of MnS thin films 148, 114821.https://doi.org/10.1016/j.optmat.2023.114821

Amri, A., Arab, L., Meftah, A., Latif, A. (2023). Effect of aluminum doping on the structural, optical and electrical properties of ZnO thin films processed under thermal shock conditions Results in Optics, 11, 100426 https://doi.org/10.1016/j.rio.2023.100426

Chaki, S. H., Chauhan, S. M., Tailor, J. P., and Deshpande, M. P. (2017). Synthesis of manganese sulfide (MnS) thin films by chemical bath deposition and their characterization. *Journal of Materials Research and Technology*, 6, 2, 123-128. https://doi.org/10.1016/j.jmrt.2016.05.003

Chowdhury, I., Podder, M. R., Islam, B. M. (2011). Synthesis and characterization of manganese sulphide thin films deposited by spray pyrolysis. *Crystal Research and Technology*, *46*, 3, 267-271. https://doi.org/10.1002/crat.201000549

Ghazai, A.J., Salmanb, E. A., Jabbar, Z.A.(2016). Effect of Aluminum Doping on Zinc Oxide Thin Film Properties Synthesis by Spin Coating Method *American Scientific Research Journal for Engineering, Technology, and Sciences Volume* 3, 202-211

Hannachi, A., Segura, A., and Maghraoui-Meherzi, H. (2016). Growth of

manganese sulfide (α-MnS) thin films by thermal vacuum evaporation: Structural, morphological and optical properties. *Materials Chemistry and Physics*, 181, 326-332. https://doi.org/10.1016/j.matchemphys.2016.06.066

Hassanzadeh, F. Z., Islam, S. M., Kanatzidis, M. G. (2015). Porous amorphous chalcogenides as selective adsorbents for heavy metals *Journal of Chemistry of Materials* 27, 18, 6189-6192

Ijeh, R., Asarhasa, P., Aisida, S.O., Ikhioya, I. L. (2023). Influence of manganese molarity incorporation on manganese silver sulphide semiconductor material for photovoltaic applications *Results in Optics* 12, 1-7, 100464

Imran, M., Afzal, A. M., Iqbal, M. W., Hegazy, H., Iqbal, M. Z., Mumtaz, S., and Qureshi, R. (2023). Manganese (Sulfide/Oxide) based electrode materials advancement in supercapattery devices. *Materials Science in Semiconductor Processing*, *158*, 107366. https://doi.org/10.1016/j.mssp.2023.107366

Imran, M., Afzal, A. M., Iqbal, M. W., Hegazy, H., Iqbal, M. Z., Mumtaz, S., and Qureshi, R. (2023). Manganese (Sulfide/Oxide) based electrode materials advancement in supercapattery devices. *Materials Science in Semiconductor Processing*, *158*, 107366. https://doi.org/10.1016

Javed, S., Suo, G., Mu, R., Lin, C., and Li, J. (2024). Progress and strategies in transition metal chalcogenides as anode for potassium-ion batteries. *Journal of Energy Storage*, *97*, 112781. https://doi.org/10.1016/j.est.2024.112781

Jeyamalar, K., and Selvarajan, P. (2021). Studies of magnesium doped Mns nanomaterial synthesized by microwave-assisted solution method. *Journal of Advanced Scientific Research*, *12*, 4, 185-192. https://doi.org/10.55218/JASR.s12021112420

Licardo, J.T., Domjan, M., Orehovaˇcki, T. (2024). Intelligent Robotics—A Systematic Review of Emerging Technologies and Trends. Electronics, 13, 542. https://doi.org/10.3390/electronics13030542

Liu, A., Zhang, X., Liu, Z., Li, Y., Peng, X., Li, X., Qin, Y., Hu, C., Qiu, Y., Jiang, H., Wang, Y., Li, Y., Tang, J., Liu, J., Guo, H., Deng, T., Peng, S., Tian, H., Tian-Ling Ren. (2024). The Roadmap of 2D Materials and Devices Toward Chips Advanced Materials Nano-Micro Letters16:119

Moreno-García, H., Sigala-Valdez, J., Martínez-Blanco, M. D. R., Cruz Reyes, I., Durón-Torres, S., Escalante-García, I., and Del Rio-De Santiago, A. (2024). Effect in variation of the cationic precursor temperature on the electrical and crystalline properties of MnS growth by SILAR. *Heliyon*, 10, 4, e26703. nano and micro architectures: synthesis, characterization and optical properties, Materials Research Bulletin 46, 1804e1810

Onwuemeka, J. I., Ndubueze, D. N., Ebosie, N. P., Nwokeke, U. G., Godwin, R. C., Nwaemene, I. M., Ogbonna, L. T., and Anozie, V. C. (2024). Dual solution synthesis of Al doped CuS thin films for optoelectronic and photovoltaic applications *World Journal of Advanced Research and Reviews*, 22, 02, 1535–1542 https://doi.org/10.30574/wjarr.2024.22.2.1499

Pandey, G., Sharma, H.K., Srivastava, S.K., Srivastava, R.K., Kotnala, R.K. (2011). γ-MnS nano and micro architectures:

synthesis, characterization and optical properties, Mater. Res. Bull. 46, 1804e1810.

Pathan, H., Kale, S., Lokhande, C., Han, S., and Joo, O. (2007). Preparation and characterization of amorphous manganese sulfide thin films by SILAR method. *Materials Research Bulletin*, 42, 8, 1565-1569. https://doi.org/10.1016/j.materresbull. 2006.11.017

Petrakovsk, G. A., Ryabinkina, L. I., Abramova, G. M., Velikanov, D. A., and Bovina, A. F. (2001). Antiferromagnet–Ferromagnet Transition in α-Mn*x*S Manganese Sulfides *Physics of the Solid State*, 43, 3, 493–495.

Tiwari, P., Jaiswal, J., and Chandra, R. (2019). Optical and electrical properties of highly ordered α-, γ- and α + γ-MnS films deposited by reactive sputtering technique *Journal of Applied Physics*, 126, 213108 (2019); doi: 10.1063/1.5127004

Wang, S; Li, .; Zhai, R; Wang, H; Hou, Y; Yan, H. (2005,). Synthesis of metastable γ-manganese sulfide crystallites by microwave irradiation. *Journal of Materials Chemistry and Physics*. 91, 298−300

Xaba, T., Al-Shakban, X., (2020). Formation of the green stable α-Mns with metastable γ-Mns nanoparticles and thin films by homogeneous precipitation route Chalcogenide Letters, 17, 8, 417 – 422

Yu, X; Li-yun, C; Jian-feng, H; Jia, L; Jie, F; Chun-yan, Y. (2013). Influence of S/Mn molar ratio on the morphology and optical property of γ-MnS thin films prepared by microwave hydrothermal. *Journal of Alloys Compound*, 549, 1−5.

Zhang, F., Cho, M., Eom, T., Kang, C., and Lee, H. (2019). Facile synthesis of manganese cobalt sulfide nanoparticles as high-performance supercapacitor electrode. *Ceramics International*, *45*, 16, 20972-20976. https://doi.org/10.1016/j.ceramint.2019.06.240

Zhang, J., Shi, R., Zhang, C., Li, L., Mei, J and Liu, S. (2018). Solvothermal synthesis of manganese sulfides and control of their phase and morphology *Journal of Materials Research, 2018, 1-9 DOI: 10.1557/jmr.2018.365*

Zhang, Y.; Wang, H.; Wang, B.; Yan, H.; Yoshimura, M. (2002). Low temperature hydrothermal synthesis of pure metastable γ-manganese sulfide (MnS) crystallites. Journal of Crystal Growth, 243, 214−217

Zhao, Y., Yao, Q., Liu, P., and Liu, Q. (2024). Accurate polymorphous description of the paramagnetic phases in MnBi2Te4. *Computational Materials Today*, 2-3, 100007. https://doi.org/10.1016/j.commt.2024.100007

Zhao, J., Wang, J., Chen, Z., Ju, J., Han, X., Deng, Y.(2021). Metal chalcogenides: An emerging material for electrocatalysis. APL Mater. 9, 5, 50902

Zheng, Y., Cheng, Y., Wang, Y., Zhou, L., Bao, F., Jia, C. (2006). J. Phys. Chem. B 110, 8284